Kinetics of precipitation in Al–Sc alloys and low temperature solid solubility of scandium in aluminium studied by electrical resistivity measurements

Hyung-Ho Jo

Foundry Technology Division, Production Technology Center, Korea Academy of Industrial Technology, 472 Kajwa-4 Dong, Seo-ku, Inchon 404-254 (South Korea)

Shin-Itiroh Fujikawa

Department of Materials Science, Faculty of Engineering, Tohuku University, Sendai 980 (Japan)

(Received April 5, 1993)

Abstract

The precipitation kinetics of Al_3Sc phases in Al–0.090at.%Sc and Al–0.15at.%Sc alloys were investigated in the aging temperature range from 533 to 733 K mainly by electrical resistivity measurements. The average Sc concentration c_{Sc} of the Al-rich matrix was calculated from the value of the resistivity. The results of aging time dependence of c_{Sc} and fraction of solute transformed were analysed from the viewpoint of time scaling, the Johnson–Mehl–Avrami equation and the Ostwald ripening theory. The rapid growth stage of the Al_3Sc phases was successfully scaled and nearly characterized by the model of diffusion-controlled growth of a fixed number of particles. The solid solubilities of Sc in aluminium from 733 K down to 643 K were estimated by the analysis of c_{Sc} of the Al-rich matrix during the Ostwald ripening of the Al_3Sc precipitates.

1. Introduction

It is well known that transition metals have a small solid solubility and a low diffusivity in aluminium, but a small amount of transition metal exerts a pronounced influence on the structure and properties of pure aluminium and of Al alloys.

Recently, it has been noted that scandium, whose maximum solid solubility in aluminium is 0.21 at.% [1, 2], produces an excellent age-hardening effect in Al–Sc alloys [3]. The maximum net increase $\Delta\sigma_{0.2}/\Delta c$ in yield stress after aging subtracted from that in the as-quenched state per unit concentration in Al–Sc alloys has the second-highest magnitude, about 1 GPa at.% [3] of all Al alloys; the value of $\Delta\sigma_{0.2}/\Delta c$ for an Al–0.027at.%Au alloy has the highest magnitude, about 2 GMPa at.% [4] and the values of $\Delta\sigma_{0.2}/\Delta c$ in the usual age-hardenable alloys are below 200 MPa at.% [3]. Moreover, the addition of Sc to other Al alloys introduces superplastic behaviour and a higher strength level with higher ductility [5, 6]. The source of this interesting behaviour is the presence of very fine equilibrium Al_3Sc precipitates which exist with coherency strain in an ordered $L1_2$ structure. On the contrary, the development of Al-based age-hardenable alloys for high temperatures is generally limited by the non-equilibrium nature of the Guinier–Preston (GP) zones and intermediate precipitates. One possible method of overcoming the difficulties is to use an alloying addition in which the precipitate is either coherent or semicoherent in its equilibrium structure. Therefore it is very important to investigate the kinetics of precipitation of the equilibrium phase in Al–Sc alloys, but detailed studies have not yet been reported.

Generally, the resistivity of an aged dilute alloy can be converted into the average concentration of solute in the matrix when the size and volume fraction of precipitates are sufficiently large and low respectively and the deviation [7] from Mattiessen's rule is negligibly small.

In the present work, the precipitation kinetics in Al–Sc alloys were investigated in detail by converting the value of the resistivity into the average Sc concentration c_{Sc} of the Al-rich matrix. Moreover, the solid solubility for Sc in aluminium at temperatures lower than 733 K was estimated by the analysis of c_{Sc}, which is associated with the Ostwald ripening process of the precipitates. This method is very effective for the determination of solid solubilities at lower temperatures where traditional methods cannot be used because of the low diffusion rate of solute. This idea

0921-5093/93/$6.00

© 1993 - Elsevier Sequoia. All rights reserved

has been successfully applied to studies of the precipitation kinetics of and determination of solid solubilities in Al-Li [8], Al-Si [9] and Al-Ge alloys [10] by Fujikawa *et al.*

2. Experimental procedures

2.1. Sample preparation

The Al-Sc master alloy containing 2.1 mass% was prepared by melting 99.9996 mass% Al in a high purity alumina crucible and then adding 99.9 mass% Sc wrapped in high purity Al foil in an atmosphere of pure argon. The melt was thoroughly stirred before pouring and was cast into a pre-heated iron mould. The Al-Sc alloys of desired composition were prepared by dilution of the master alloys with high purity Al. The ingots 20 mm in diameter were homogenized at 573 K for 7 ks and formed into wires of 0.5 mm diameter by cold swaging and drawing. According to the result of the chemical analysis, the concentrations of Sc and impurities were as follows: 0.10 mass% (0.060 at.%), 0.15 mass% (0.090 at.%), 0.20 mass% (0.12 at.%) and 0.25 mass% (0.15 at.%) Sc; 0.006 mass% Mg, 0.004 mass% Fe, 0.001 mass% Cu and 0.001 mass% Si.

2.2. Electrical resistivity measurement and thermal treatment

The specimen for the resistivity measurement was mounted on a quartz specimen holder. The high purity Al wires of 0.5 mm diameter were spot welded to the specimens as potential leads. The distance between the potential leads on the specimen was about 0.4 m. Both ends of the specimen itself were used as current leads. The resistivity was measured at 77 K by the four-probe method using a precision potentiometer and a standard resistance (0.1 Ω). The measurements were repeated about ten times to obtain one data point, reversing the current direction to eliminate the stray electromotive forces. Correction for the liquid-nitrogen temperature was made with a dummy specimen. The distance between potential leads was measured using a precision scale. The diameter of the specimen was measured at different positions and the average value was evaluated. From these results the specific electrical resistivity was calculated. The resistivity was determined to an accuracy of 2 part in 10^3. The specimens were homogenized in air at 913 K for 3.6 ks in a horizontal furnace and quenched into iced water. The quenched alloys were isothermally aged at various temperatures between 533 and 733 K. Aging was carried out in an electrical furnace in air.

2.3. Hardness measurement

Microhardness tests were carried out using the Vickers method. The indentation was made on the well-polished surface of the disc-shaped specimens with a diamond square-based pyramid under a load of 0.5 kgf for a period of 20 s. The measurements were repeated eight times and the mean value was calculated.

2.4. Transmission electron microscopy

Strips of specimens were cold rolled to 0.2 mm in thickness, allowing thinning for transmission electron microscopy (TEM). The samples for TEM were prepared by twin-jet polishing in an electrolyte solution consisting of 90% nitric acid and 10% water. TEM was carried out using an electron microscope of the JEOL-200 B type.

3. Results

3.1. Hardness change

Figures 1 and 2 show the hardness change plotted as a function of aging time for the Al-0.15at.%Sc and Al-0.090at.%Sc alloys respectively. A maximum like a plateau was observed. The maximum hardness and the

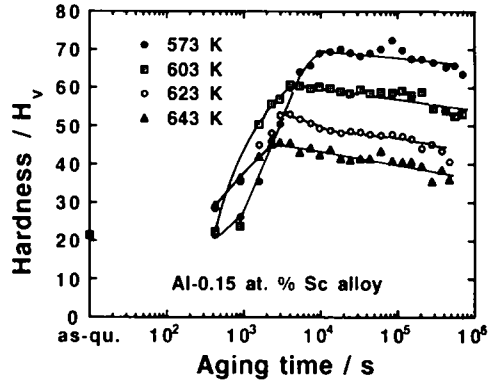

Fig. 1. Age-hardening curves for the Al-0.15at.%Sc alloys.

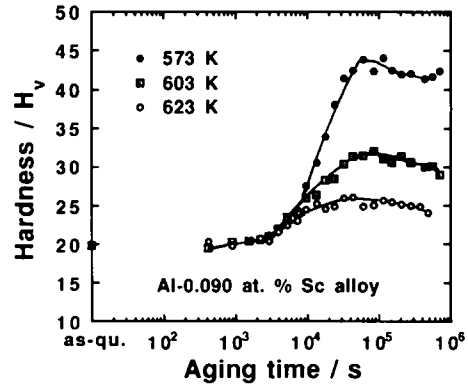

Fig. 2. Age-hardening curves for the Al-0.090at.%Sc alloys.

aging time taken to reach the maximum hardness depended greatly on the aging temperature and Sc concentration. The maximum hardness H_V^{max} and the time taken to reach the maximum hardness were smaller and longer respectively with decrease in Sc concentration. The highest H_V^{max} was obtained after aging at 573 K. This aging temperature is much higher than in usual age-hardenable Al alloys. According to the results of Dritz *et al.* [3], the age hardening in Al–Sc alloys was scarcely observed after aging even for a long time at lower temperatures than 473 K. On the contrary, for dilute Al–Au alloys [4], value of H_V^{max} was obtained after aging at 393 K. This difference between the characteristics of age hardening of the two alloys can be attributed to the difference between the diffusion rates of these solutes and the mechanism of age hardening. Another prominent feature of the age hardening of Al–Sc alloys is the high degree of resistance to softening and the high hardness level retained for a long aging time, as shown in Figs. 1 and 2. This suggests that the coherency of the precipitates is fairly stable as would be expected from the fact that they are in their equilibrium state and the diffusion rate of Sc in aluminium is low [11].

3.2. Transmission electron microscopy

Figure 3(a) shows the typical microstructure of the aged Al–0.15at.%Sc alloy. This specimen was aged at 573 K for 600 ks, corresponding to the overaging stage shown in Fig. 1. Very fine precipitates are homogeneously dispersed in the matrix. Figure 3(b) shows the electron diffraction pattern of the same specimen used in Fig. 3(a). Strong superlattice reflections were observed. It was recognized from Fig. 3 that the precipitates are the Al_3Sc phase with the $L1_2$ structure. Figure 3(a) shows the coffee-bean-like strain contrast explained by the Ashby–Brown [12] model; a large coherency strain exists near the precipitates. Similar phenomena have been reported for the equilibrium precipitates in Cu–Co alloys [13]. The large coherency strain is attributed to the large difference between the lattice parameters of the Al_3Sc phase and Al matrix and is the origin of the large degree of age hardening in Al–Sc alloys. Figure 3(a) shows that the coherency strain is still maintained after aging for a longer aging time; hence the stable coherency is one cause of the small softening as opposed to overaging.

3.3. Resistivity change

Figures 4 and 5 show the resistivity plotted as a function of aging time for the Al–0.15at.%Sc and Al–0.090at.%Sc alloys respectively. The resistivity decreases with increase in the aging time. The decrease corresponds to the decrease in c_{Sc} in the Al-rich matrix

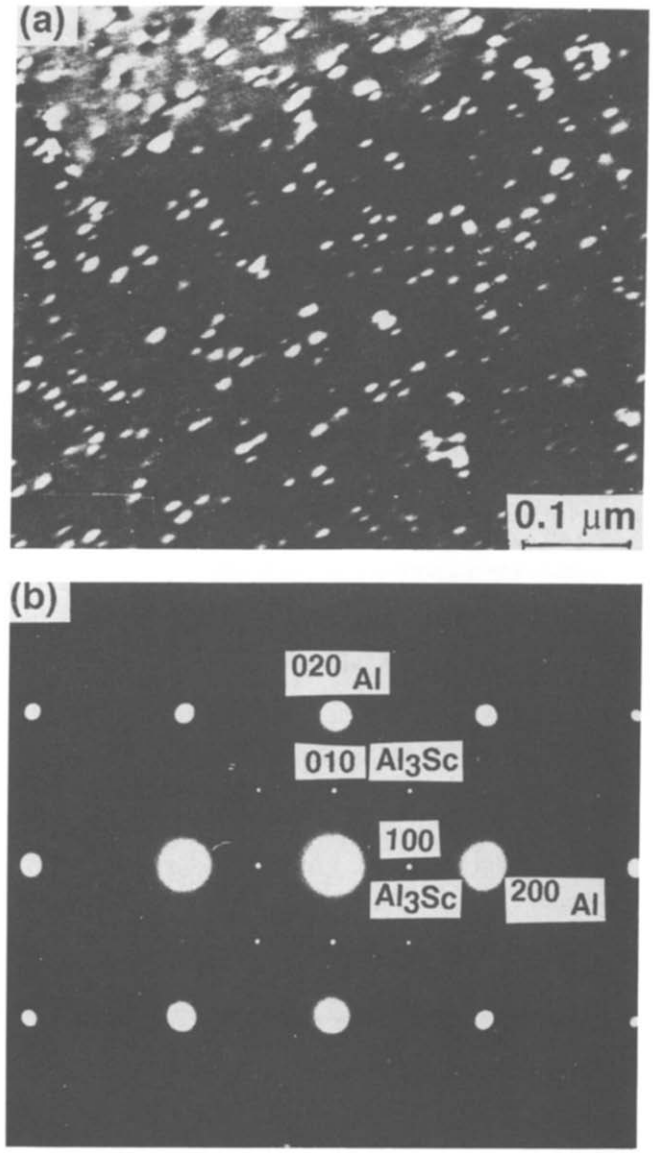

Fig. 3. (a) Dark field transmission electron micrograph of Al_3Sc particles in the Al–0.15at.%Sc alloy aged at 573 K for 600 ks and (b) (001)-oriented electron diffraction pattern from the Al_3Sc particles.

owing to the nucleation and growth of Al_3Sc precipitates. The change in the resistivity shown in Figs. 4 and 5 can be roughly divided into three stages in view of the precipitation process: an early stage with an incubation period, a rapid growth stage, and a gradual growth stage with the Ostwald ripening process. The early stage was very short in the Al–0.15at.%Sc alloy and was clearly observed in the Al–0.090at.%Sc alloy. The end time t_E of the rapid growth stage, as shown in Fig. 4, was shorter with increases in aging temperature and Sc concentration. Figure 6 shows the concentration dependence of the difference between the resistivities of the Al–Sc solid solution and the resistivity (2.297 nΩ m) of pure aluminium obtained in the present work

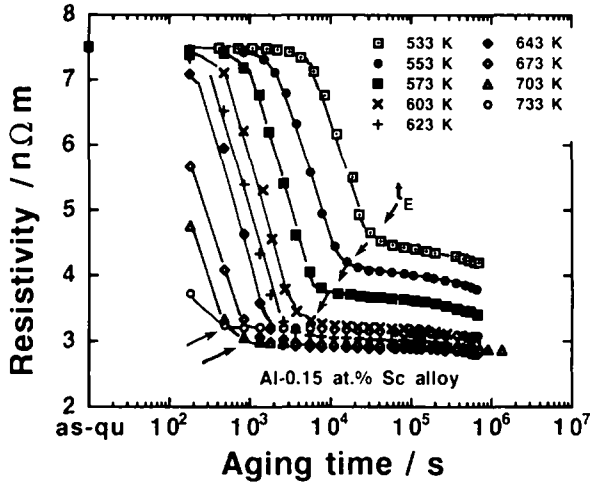

Fig. 4. Resistivity plotted against aging time in the Al-0.15at.%Sc alloys. The end times t_E of the rapid growth stage are indicated by the arrows.

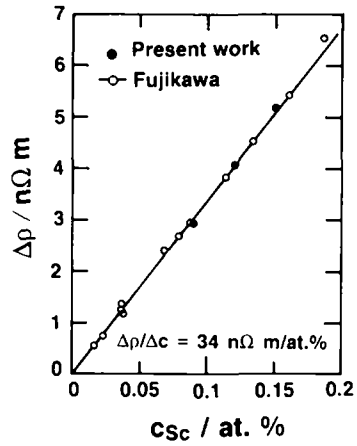

Fig. 6. Resistivity increment of the Al-Sc alloy as a function of Sc concentration in solid solution. The present work is compared with the results of Fujikawa *et al.*

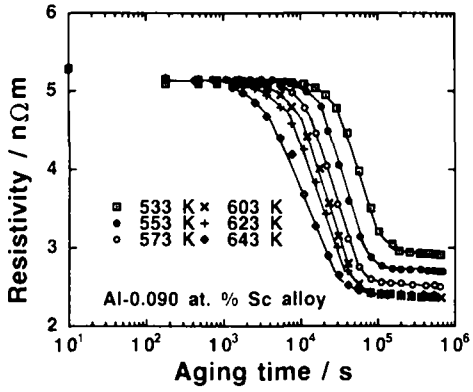

Fig. 5. Resistivity plotted against aging time for the Al-0.090at.%Sc alloys.

in comparison with the result of Fujikawa *et al.* [2]. The data in the present work were in good agreement with the result reported by Fujikawa *et al.* Figure 6 shows that the resistivity increment is linearly proportional to the Sc concentration over a wide range of concentrations. Generally, in determining the average solute concentration in the matrix from the resistivity of aged specimens, it is necessary that the magnitude $\Delta(T, c)$ of the deviation [7] from Mattiessen's rule is negligibly small, the contribution to resistivity from precipitates can be ignored, and the resistivity increment must be linearly proportional to solute concentration in the matrix. The value of $\Delta(T, c)$ for the Al-Sc alloy is not yet known. However, as shown in Fig. 6, the resistivity increment caused by Sc atoms in the solid solution is linearly proportional to the Sc concentration and the straight line determined by the least-squares method passes through the origin; hence, the value of $\Delta(T, c)$ is negligibly small. The average size of Al_3Sc particles, except in the early stage of the present work, was larger than 10 nm according to electron microscopy studies in the present work and by other workers [3, 14], and the volume fraction of the Al_3Sc precipitates is, of course, very low because it is a dilute alloy; therefore, the distance between the Al_3Sc precipitates was sufficiently large in comparison with the mean free path of an electron in aluminium. Figure 4 in ref. 2 shows that the resistivity hardly depends on the Sc concentration beyond the solid solubility; consequently, the contribution to the resistivity from the Al_3Sc precipitates can be neglected in the resistivity of the Al-Sc alloys. These results furnish a satisfactory basis for our analytical method used to measure the average Sc concentration in the matrix. The value of 34 nΩ m at.%$^{-1}$ determined by Fujikawa *et al.* [2], shown in Fig. 6, was used in the present work as the resistivity increment $\Delta\rho/\Delta c$ per atomic per cent of Sc in the solid solution of the Al-Sc alloys. The value is in good agreement with the value of 35 nΩ m at.%$^{-1}$ obtained by Ocko *et al.* [15]. Moreover, some influence of lattice strain due to the coherent Al_3Sc precipitates is possible, but in the present work this was neglected. Figures 7 and 8 show the time variation in the average Sc concentration of the Al matrix calculated using the results shown in Figs. 4 and 5 and the value of $\Delta\rho/\Delta c$, indicating that the precipitation rate in the Al-0.090at.%Sc alloy is slower than that in the Al-0.15at.%Sc alloy owing to the low supersaturation of the solute.

4. Discussion

4.1. Precipitation process in Al-Sc alloys

Evidence of the existence of GP zones and any metastable precipitates, except equilibrium Al_3Sc

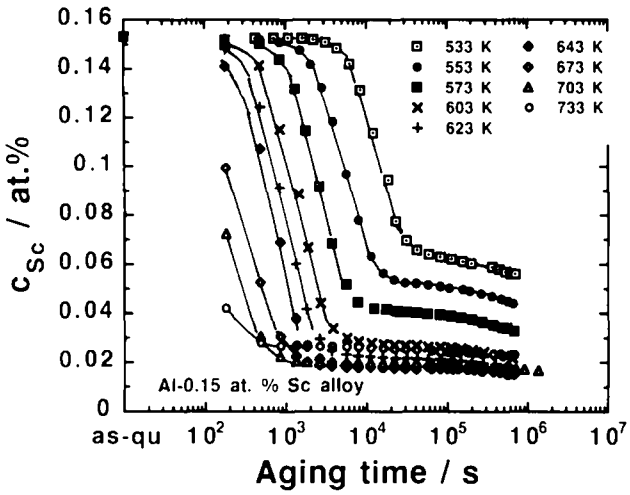

Fig. 7. Average Sc concentration in the matrix against aging time for the Al-0.15at.%Sc alloys.

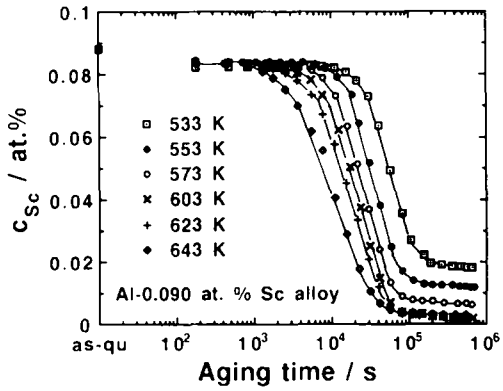

Fig. 8. Average Sc concentration in the matrix against aging time for the Al-0.090at.%Sc alloys.

precipitates, were not obtained by TEM in the present work and other studies [3, 14], by field ion microscopy (FIM) [16] and by the resistivity measurements in the present work. The Al_3Sc phases and ordering observed in Al-Li alloys were not found in the as-quenched state. The precipitation process in the Al-Sc alloys is comparatively simple. However, interestingly the equilibrium spherical Al_3Sc phases maintain a large coherency strain for a long aging time according to the TEM results of the present work and other studies [3, 14] and to FIM [16]; the large amount of age hardening originates in the coherency strain. Non-coherent Al_3Sc phases were expected to precipitate from the beginning of aging above the critical aging temperature from the results of hardness and resistivity measurements. Figure 9 shows the time $t_{F=0.5}$ and t_E in Al-0.15at.%Sc and Al-0.090at.%Sc alloys plotted against the reciprocal of aging temperature, where $t_{F=0.5}$ is the time taken to reach the stage where half the fraction of atoms are transformed as described in Section 4.2 and t_E is the end time of the rapid growth stage described in Section 3.3. This plot gives the so-called C curves in the Al-0.15at.%Sc alloy and cannot be expressed by a single straight line over a wide range of aging temperatures; the C curves consist of two branches interpenetrating each other. The result can be explained by supposing that the upper branch represents the non-coherent Al_3Sc precipitates and the lower branch represents the coherent Al_3Sc precipitates. Corresponding to this result, at aging temperatures higher than 643 K, the magnitude of the age hardening was smaller and the softening due to overaging was larger than that at lower aging temperatures. However, the question arises whether the coherent Al_3Sc phase must be distinguished from the non-coherent Al_3Sc phase or not as different phases. Figure 9 shows also that the reaction rate in the Al-0.090at.%Sc alloy is much lower than that in the Al-0.15at.%Sc alloy.

4.2. The Ostwald ripening of Al_3Sc precipitates and the solid solubility of Sc in aluminium

According to the often adopted Lifshitz-Slyozov-Wagner (LSW) theory [17, 18] and the LSW theory of diffusion-controlled coarsening modified by Ardell [19, 20], the average concentration c of solute in the matrix during coarsening of precipitates varies asymptotically with aging time t as

$$c - c_e = (\kappa t)^{-1/3} \tag{1}$$

where c_e is the equilibrium concentration of solute in equilibrium with a precipitate of infinite size and the rate constant κ is given by

$$\kappa = \frac{D(RT)^2}{9\sigma^2 e^2 V_m} \tag{2}$$

where D is nearly equal to the diffusivity of solute in the matrix, RT has its usual meaning, σ is the interfacial free energy of the precipitate-matrix interface and V_m is the molar volume of the precipitate particle. If the experimentally determined values of c are plotted as a function of $t^{-1/3}$, a linear relationship should exist at sufficiently long aging times, and the equilibrium concentration c_e can be obtained directly by extrapolation to $t^{-1/3} = 0$ ($t = \infty$). Figure 10 shows the time variation in c_{Sc} from Fig. 7 in the stage corresponding to the Ostwald ripening of the Al_3Sc precipitates in the Al-0.15at.%Sc alloy, where the mean radius of the Al_3Sc particles is proportional to $t^{1/3}$, according to electron microscopy results [3, 16, 21]. The experimentally measured values of c in mole per cubic metre ($10^{-2}\rho W_{Sc} M_{Sc}$) are plotted against $t^{-1/3}$ in Fig. 10, where $\rho = 2700$ kg m^{-3} is the density of the solid solution, and W_{Sc} and M_{Sc} are the Sc concentration in mass

per cent and the molar mass of Sc respectively. The values of c_e were determined using the least-squares method. The values of c_e and κ are shown in Table 1. The rate constant obtained from the coarsening data in Fig. 10 can be used to calculate the value of σ, provided that the solute diffusion data are known. The value of σ was determined in the present work using the experimental values of κ and the impurity diffusivity of Sc in Al [11] using eqn. (2). Then the molar volume of the Al_3Sc precipitates was calculated from the relationship $V_m = Na^3$, where N is Avogadro's number and a (= 0.4105 nm [22]) is the lattice constant of the unit cell of Al_3Sc. The value of V_m is thus 4.17×10^{-5} m^3 mol^{-1}. We calculated the value of D in eqn. (2) using the values of D_0 and Q for the impurity diffusion of Sc in aluminium [11]. The calculated values of σ are given in Table 1. The values of σ range from 40 to 60 mJ m^{-2}; the magnitude for the Al_3Sc phases is smaller than that [9] for the equilibrium non-coherent Si precipitates in Al–Si alloys and larger than that [19] for the intermediate coherent γ' phases with the $L1_2$ structure in Ni–Al alloys; hence, the values for the Al_3Sc phase are reasonably small.

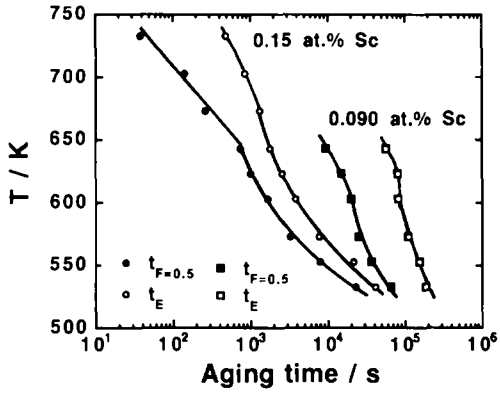

Fig. 9. C curves obtained from the time $t_F = 0.5$ and the end time t_E of rapid growth in the Al–0.15at.%Sc and Al–0.090at.%Sc alloys.

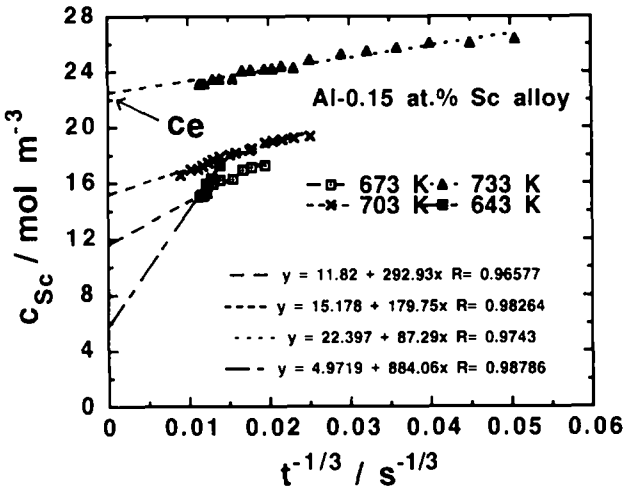

Fig. 10. Variation in average Sc concentration of the Al-rich matrix as a function of $t^{-1/3}$ during the coarsening of the Al_3Sc precipitates in the Al–0.15at.%Sc alloys. The value of c_e, obtained by extrapolation of $t^{-1/3}$, is indicated.

Thermodynamically, for a dilute solid solution, the variation in solid solubility with temperature is given by

$$C = \exp\left(\frac{\Delta S}{R}\right) \exp\left(-\frac{\Delta H}{RT}\right) \qquad (3)$$

where C is the solid solubility in atomic per cent, ΔS is the excess entropy of mixing, ΔH is the heat of mixing and RT has its usual meaning. Figure 11 shows the logarithm of the values of c_e in the present work as a function of the reciprocal temperature, in comparison with the solid solubilities of Sc in aluminium determined by Fujikawa *et al.* [2] and Dritz *et al.* [23]. Applying the result of the present work in Fig. 11 to eqn. (3), the values of $\Delta S/R$ and ΔH were calculated by the least-squares method to be 6.57 and 62.8 kJ mol^{-1} respectively. The results were in good agreement with the values obtained by Fujikawa *et al.* ($\Delta S/R = 6.02$ and $\Delta H = 58.5$ kJ mol^{-1}). The extrapolated solubility line of the present work, as shown in Fig. 11, agrees well with the solid solubilities above 833 K by Fujikawa *et al.*

TABLE 1. Values of the rate constant κ, the equilibrium solid solubility c_e and the interfacial free energy determined from coarsening data for Al–Sc alloys

T (K)	c_e (mol m^{-3} (at.%))	κ (m^9 m^{-3} s^{-1})	D^* (m^2 s^{-1})	σ (J m^{-2})
733	22.4 (2.24×10^{-2})	1.50×10^{-6}	1.30×10^{-17}	4.13×10^{-2}
703	15.2 (1.52×10^{-2})	1.72×10^{-7}	1.74×10^{-18}	6.32×10^{-2}
673	11.8 (1.18×10^{-2})	3.97×10^{-8}	1.95×10^{-19}	5.42×10^{-2}
643	4.97 (4.97×10^{-3})			

[a]The diffusivity D was calculated using the values of D_0 and Q for the impurity diffusion of Sc in aluminium obtained by Fujikawa *et al.* [11].

4.3. Kinetics and scaling of precipitation in Al-Sc alloys

Here, we have calculated the fraction F of solute transformed by time t using the results shown in Figs. 7 and 8 and thereby discussed the kinetics of precipitation in the Al-0.15at.%Sc and Al-0.090at.%Sc alloys. F is expressed by the following equation:

$$F = \frac{c_0 - c_t}{c_0 - c_e} \tag{4}$$

where c_0 is the concentration of solute in solution at zero aging time, c_t is the concentration at aging time t, and c_e is the equilibrium concentration. The values of c_e at 643, 673, 703 and 733 K were given by the results in Table 1 and the values at other temperatures below 623 K were calculated using eqn. (3) and the values of $\Delta S/R$ and ΔH from the present work. Figures 12 and 13 show the aging time dependence of F calculated in this way for the Al-0.15at.%Sc and Al-0.090at.%Sc alloys respectively. Most of the results gave sigmoidal curves for F against aging time, where the value of F increases slowly at first, then much more rapidly and finally slowly again. For the Al-0.090at.%Sc alloys, the three stages were clearly observed at all aging temperatures. On the contrary, for the Al-0.15at.%Sc alloys, the reaction rate was very large owing to the higher supersaturation of solute; for aging temperatures higher than 623 K, at short aging times more than 80% of transformation was finished and it was difficult to detect the three stages. The time taken to reach $F = 0.5$ in Al-0.15at.%Sc has already been plotted against the reciprocal aging temperature in Fig. 9.

It is very important to investigate the scaling properties using a normalizing parameter for the kinetics of phase decomposition and to find the universal law of self-similar evolution of the decomposition process [24]. There are generally two aspects to the scaling of phase decomposition. One is structural scaling, which has been investigated mainly by small-angle X-ray and neutron scattering, and where the configuration of the particle distribution remains the same except for the aging-time-dependent characteristic scaling length. The second is time scaling, from which a universal time scale may be deduced to evaluate the precipitation kinetics, independently of aging time, aging temperature and composition. In the present work, the aging time was normalized by an appropriate time, and time scaling was investigated. Figures 14 and 15 show the time scaling of the results shown in Figs. 12 and 13. The aging time was normalized by the time taken to reach $F = 0.5$. The value of F itself can also be said to be the magnitude obtained by scaling the solute concentra-

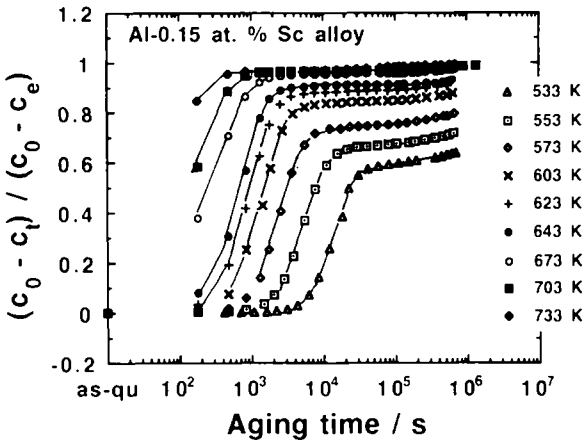

Fig. 12. Fraction of the solute transformed in the Al-0.15at.%Sc alloys against aging time.

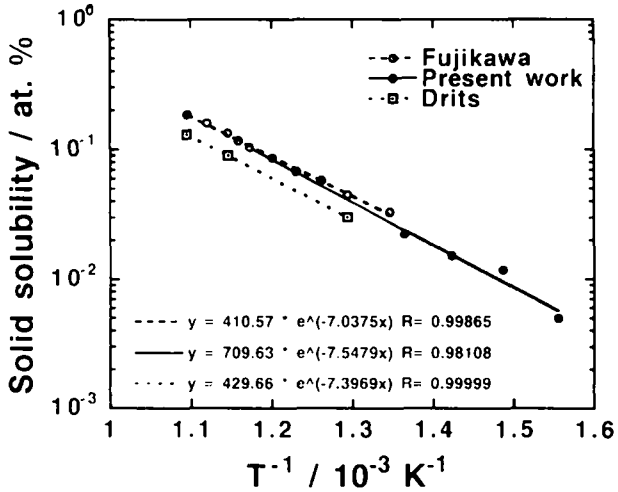

Fig. 11. Comparison of c_e obtained in the present work with the solid solubilities of Sc in aluminium obtained by other workers.

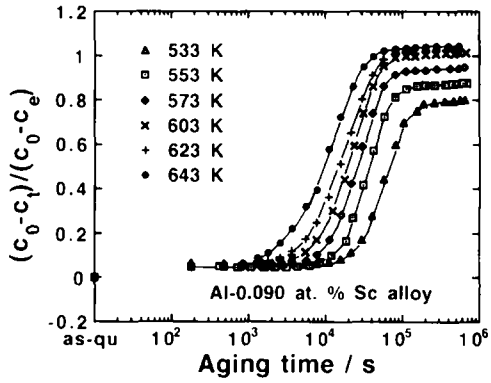

Fig. 13. Fraction of the solute transformed in the Al-0.090at.%Sc alloys against aging time.

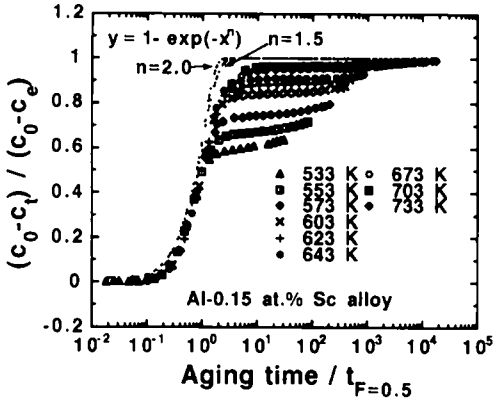

Fig. 14. Time scaling for the fraction of the solute transformed in the Al-0.15at.%Sc alloys. The aging time is scaled by the time to reach $F=0.5$.

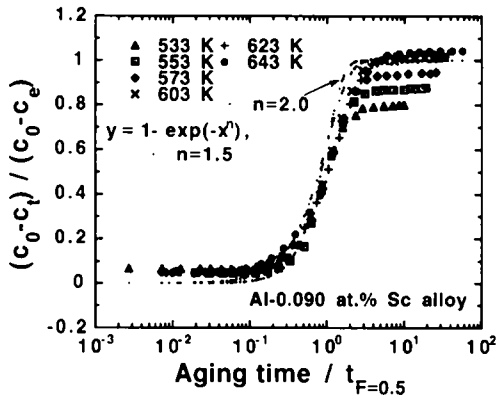

Fig. 15. Time scaling for the fraction of the solute transformed in the Al-0.090at.%Sc alloys. The aging time is scaled by the time to reach $F=0.5$.

tion. It is noted that the values of F in the initial stage and the rapid stage at temperatures below 673 K and the values in all the stages at temperatures above 673 K fall on one master curve; hence, the early stage and the rapid growth stage are excellently scaled, independent of aging time, aging temperature and Sc content. Consequently, the decomposition at the early stage and the rapid growth stage of precipitation in the Al-Sc alloys can be controlled by the universal law, independent of aging temperature, aging time and solute concentration. However, the gradual stage with the Ostwald ripening process at temperatures below 643 K did not conform to this time scaling. The reason has not been clear in the present work. The scaled curves are compared in Figs. 14 and 15 with the following scaling function:

$$y=1-\exp(-x^{1.5}) \tag{5}$$

$$y=1-\exp(-x^{2.0}) \tag{6}$$

Although some discrepancy between the experimentally scaled curve and eqn. (5) or eqn. (6) was observed, the scaled curves may be approximated by eqn. (5) or eqn. (6) in the region where F is below about 0.8. In the present work, the best scaling function over the whole range of F could not be found. Equation (5) and eqn. (6) are similar to the Johnson-Mehl-Avrami (JMA) relation [25, 26] for three-dimensional nucleation and growth as follows:

$$F=1-\exp(-kt^n) \tag{7}$$

where t is the time, and k and n are constants; k corresponds to the so-called rate constant and has the dimensions of $(\text{time})^{-n}$. Avrami [26] pointed out that, if one plots F against $\log t$, all the curves with the same value of n will have the same shape and will differ only in the value of k, which is equivalent to a change in k, corresponding to a change in scale. Here, we analysed the results shown in Figs. 12 and 13 by the JMA relation. When eqn. (7) is applied to the result of precipitation, a straight-line relation with the slope n should be found in the maximum observable experimental range of reaction. Therefore, by plotting $\log\{\log[1/(1-F)]\}$ against $\log t$, one can obtain the time exponent n. Figures 16 and 17 show the $\log\{\log[1/(1-F)]\}$ *vs.* $\log t$ plots for the Al-0.15at.%Sc and Al-0.090at.%Sc alloys respectively. The existence of a straight-line relation was observed in the rapid growth stage. The JMA exponent n below 643 K is close to $\frac{3}{2}$ for the Al-0.15at.%Sc and Al-0.090at.%Sc alloys, which means the growth of a fixed number of particles [27]. Since the reaction rate at aging temperatures above 673 K for the Al-0.15at.%Sc alloy was very large, a few data were obtained for F of the rapid growth stage; the data correspond to the stage of deviation from the JMA relation at aging temperatures below 643 K, and therefore the values of n and k were not calculated in the present work.

4.4. *Activation energy for precipitation*

Figure 18 shows the Arrhenius plots of $t_{F=0.5}$ of the linear part for the Al-0.15at.%Sc alloys in Fig. 9. The apparent activation energy was determined from the straight-line relationship between the time taken to reach $F=0.5$ and the reciprocal of absolute temperature using the following equation:

$$t_{F=0.5}=k_1\exp\left(-\frac{Q}{RT}\right) \tag{8}$$

where k_1 is a constant. The values of Q obtained are given in Table 2. No difference between Q for the upper branch and Q for the lower branch was observed. The value was much smaller than the activa-

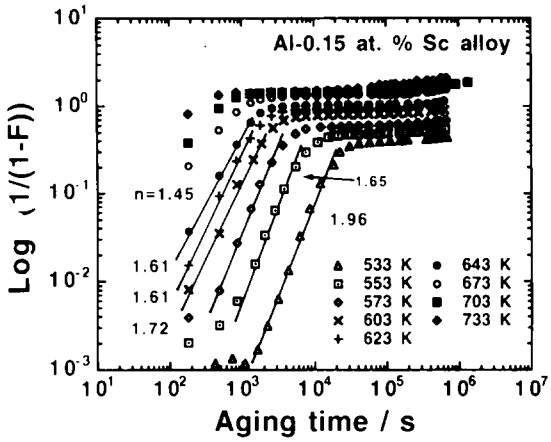

Fig. 16. JMA plot for the Al–0.15at.%Sc alloys.

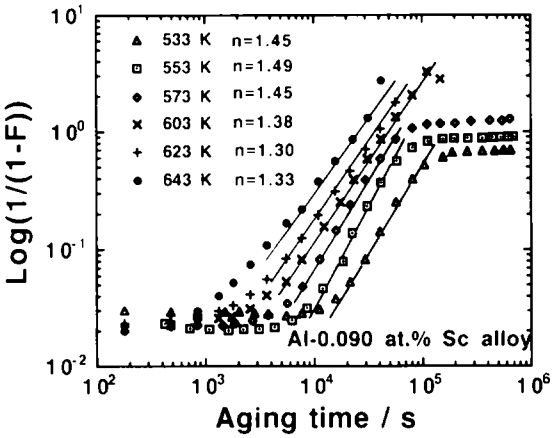

Fig. 17. JMA plot for the Al–0.090at.%Sc alloys.

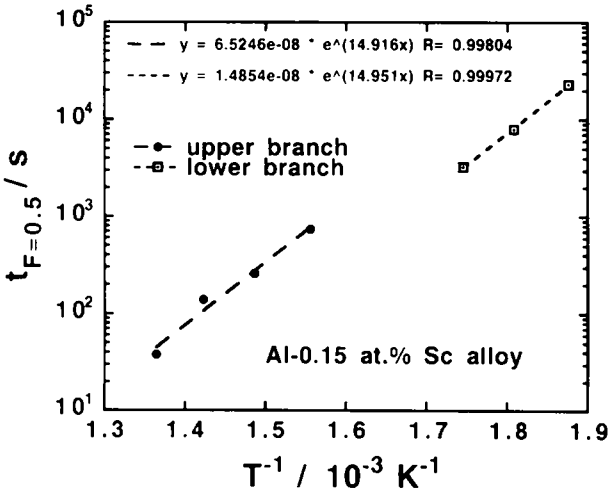

Fig. 18. Relationship between the time to reach $F = 0.5$ and the reciprocal aging temperature for the Al–0.15at.%Sc alloys.

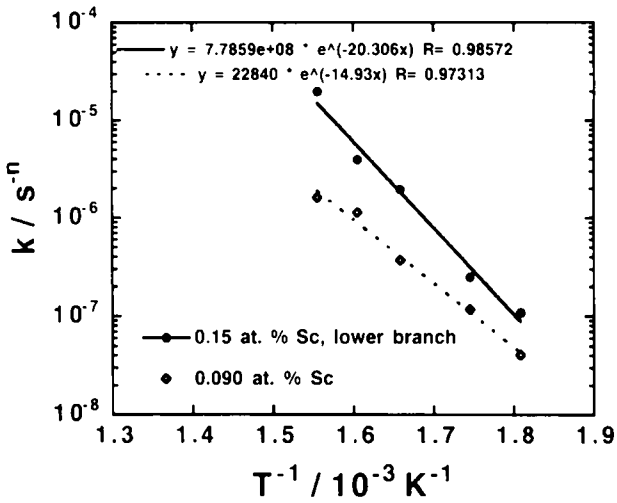

Fig. 19. Relationship between the rate constant k in the JMA equation and the reciprocal aging temperature in the Al–0.15at.%Sc and Al–0.090at.%Sc alloys.

TABLE 2. Apparent activation energy for precipitation in Al–0.15at.%Sc and Al–0.090at.%Sc alloys

Sc concentration (at.%)	Q (kJ mol^{-1})		
	643–733 K	533–573 K	553–643 K
0.15	124[a]	124[a]	169[b]
0.090			124[b]

[a]This value was determined from the temperature dependence of the time taken to reach the stage where half the fraction of atoms is transformed.
[b]This value was determined from the temperature dependence of the rate constant k in the JMA relation.

tion energy (217–286 kJ mol^{-1}) [11] for impurity diffusion of Sc and other transition metals in aluminium. Moreover, from the stage where the JMA relation is valid, the value of Q can be determined from the temperature dependence of the rate constant k:

$$k = k_2 \exp\left(-\frac{Q}{RT}\right) \tag{9}$$

where k_2 is a constant. Figure 19 shows the Arrhenius plots of the rate constant k in the JMA relation for the Al–0.15at.%Sc and Al–0.090at.%Sc alloys. The values of Q obtained using eqn. (9) are given in Table 2. The values were also smaller than the activation energy for impurity diffusion of Sc and other transition metals in aluminium. A possible explanation of the disagreement between the activation energies of diffusion and precipitation may be the high excess vacancy concentration after quenching because a strong attraction

between Sc atoms and vacancies was expected [28–30]; the activation energy for precipitation corresponds to the migration energy of a Sc atom in Al–Sc alloys. Another explanation could be the easy formation and high dispersion of Al_3Sc precipitates because of their coherency and low interfacial energy of the precipitate–Al matrix interface.

5. Conclusions

(1) The precipitation process and kinetics in Al–0.090at.%Sc and Al–0.15at.%Sc alloys were investigated by resistivity and hardness measurements, and TEM.

(2) It was found that the equilibrium Al_3Sc phases with the $L1_2$ structure precipitate homogeneously without the formation of any other metastable phases. The Al_3Sc phases maintained coherency with the matrix for a long aging time.

(3) The average Sc concentration c_{Sc} of the Al-rich matrix at aging time t was calculated from the resistivity results. The curve of c_{Sc} *vs.* log t consists of an early stage with an incubation period, a rapid growth stage, and a later stage with the Ostwald ripening process. The concentration c_e of the solute, in equilibrium with the Al_3Sc particles of infinite size, corresponding to solid solubility, was determined by extrapolating the c_{Sc} *vs.* $t^{-1/3}$ plots in the Ostwald ripening stage to infinite time as follows: 4.97×10^{-3} at.% at 643 K, 1.18×10^{-2} at.% at 673 K, 1.52×10^{-2} at.% at 703 K and 2.24×10^{-2} at.% at 733 K. From the temperature dependence of the solid solubilities, the excess entropy of mixing and heat of mixing associated with the formation of a solid solution of Sc in aluminium were calculated to be 6.57 R and 62.8 kJ mol^{-1}, respectively.

(4) The fraction F of atoms transformed at different aging times was calculated from the values of c_{Sc} and c_e. The curve of F *vs.* log t was analysed from the viewpoint of the time scaling and the Johnson–Mehl plot. It is found that most stages can be clearly scaled by one master curve. The JMA exponent n was nearly equal to $\frac{3}{2}$ in the rapid growth stage at aging temperatures lower than 643 K, corresponding to the model of diffusion-controlled growth of a fixed number of particles.

(5) The interfacial free energy of Al_3Sc was determined from the values of c_e, the rate constant κ in the equation $c - c_e = (\kappa t)^{-1/3}$ in the Ostwald ripening stage and the impurity diffusivity of Sc in aluminium by Fujikawa *et al.*

(6) The activation energies for the precipitation of Al_3Sc were determined by the temperature dependence of two kinetic parameters, showing that the values were smaller than the activation energy for impurity diffusion of Sc and other transition metals in aluminium.

Acknowledgments

One of the authors (H.-H. Jo) acknowledges Professor K. Hirano for discussions and encouragement. The other author (S.-I. Fujikawa) was supported by the Light Metal Educational Foundation Inc.

References

1 T. B. Massalski (ed.), *Binary Alloy Phase Diagrams*, Vol. 1, 2nd edn., American Society for Metals, Metals Park, OH, 1990, p. 208.
2 S.-I. Fujikawa, M. Sugaya, H. Takei and K. Hirano, *J. Less-Common Met., 63* (1979) 87.
3 M. E. Dritz, G. B. Ber, Yu. G. Bikov, G. S. Toropova and G. K. Anastasbeva, *Phys. Met. Metallogr. (Engl. Transl.), 57* (1984) 1172.
4 S.-I. Fujikawa, K. Hirano and M. Hirabayashi, *Z. Metallkd., 59* (1968) 782.
5 R. A. Emigh, E. L. Brdley and J. W. Morris, Jr., in E. W. Lee and N. J. Kim (eds.), *Light-Weight Alloys for Aerospace Applications II*, Metallurgical Society of AIME, Warrendale, PA, 1991, p. 27.
6 R. R. Sawtell and C. L. Jensen, *Metall. Trans. A, 21* (1990) 421.
7 P. L. Rossiter, *The Electrical Resistivity of Metals and Alloys*, Cambridge University Press, Cambridge, Cambs., 1987, p. 9.
8 S.-I. Fujikawa, Y. Izeki and K. Hirano, *Scr. Metall., 20* (1986) 1275.
9 S.-I. Fujikawa, Y. Oyobiki and K. Hirano, *J. Jpn. Inst. Light Met., 29* (1979) 331.
10 S.-I. Fujikawa and Y.-I. Izeki, *Metall. Trans. A, 23* (1993) 277.
11 S.-I. Fujikawa, in K. Hirano, H. Oikawa and K. Ikeda, *Science and Engineering of Light Metals*, Japan Institute of Light Metals, 1991, p. 959.
12 M. F. Ashby and L. M. Brown, *Philos. Mag., 8* (1963) 1083.
13 Y. Tomoiiyo, S. Matsumura and M. Toyohara, *J. Electron. Microsc., 34* (1985) 438.
14 A. G. Bepezina, V. A. Bogkov, B. P. Domshunikov, S. B. Ivanobv and K. V. Tsuistov, *Metallophysika, 12* (1990) 72.
15 M. Ocko, E. Babic, R. Krsmik, E. Girt and B. Leontic, *J. Phys. F, 6* (1976) 703.
16 N. Sano, Y., Hasegawa, K. Hono, H. H. Jo, K. Hirano, H. W. Pickering and T. Sakurai, *J. Phys. (Paris), Colloq. C6, 48* (1987) 337.
17 I. M. Lifshitz and V. V. Slyozov, *J. Phys. Chem. Solids, 19* (1961) 35.
18 C. Wagner, *Z. Electrochem., 65* (1961) 581.
19 A. J. Ardell, *Acta Metall., 20* (1972) 61.
20 A. J. Ardell, *Acta Metall., 15* (1967) 1772.
21 M. Nakayama, A. Yoshida and Y. Miura, *Proc. Spring Meet. of Japan Institute of Light Metals, May, 1991*, Japan Institute of Light Metals, Tokyo, 1991, p. 273.
22 N. Blake and M. A. Hopkins, *J. Mater. Sci., 20* (1985) 2861.
23 M. E. Dritz, E. S. Kadaner, T. V. Dobatkina and N. T. Turkina, *Izv. Akad. Nauk SSSR Met.* (4) (1973) 213.

24 S. Komura and H. Furukawa (eds.), *Dynamics of Ordering Process in Condensed Matter*, Plenum, New York, 1988.
25 W. A. Johnson and R. F. Mehl, *Trans. AIME, 135* (1939) 416.
26 M. A. Avrami, *J. Chem. Phys., 7* (1939) 1103; *8* (1940) 212; *9* (1941) 177.
27 J. Burke, *The Kinetics of Phase Transformations in Metals*, Pergamon, Oxford, 1965, p. 184.
28 E. Hashimoto, K. Miura, T. Kino, R. Matsushita and M. Koyama, *Jpn. J. Appl. Phys., 18* (1979) 881.
29 A. S. Berger and R. W. Siegel, *J. Phys. F, 9* (1979) L67.
30 T. Torma, E. Kovacs-Csetényi and T. Turmezey, *Defect Diffus. Forum, 66–69* (1989) 1479.